Journal of Statistical Mechanics: Theory and Experiment
An IOP and SISSA journal

Trajectory entanglement in dense granular materials

James G Puckett[1], **Frédéric Lechenault**[2], **Karen E Daniels**[1] **and Jean-Luc Thiffeault**[3]

[1] Department of Physics, NC State University, Raleigh, NC 27695, USA
[2] Laboratoires de Physique Statistique, École Normale Supérieure, 24 rue Lhomond, 75005 Paris, France
[3] Department of Mathematics, University of Wisconsin, Madison, WI 53706, USA
E-mail: jgpucket@ncsu.edu, frederic.lechenault@lps.ens.fr, kdaniel@ncsu.edu and jeanluc@math.wisc.edu

Received 23 February 2012
Accepted 24 May 2012
Published 18 June 2012

Online at stacks.iop.org/JSTAT/2012/P06008
doi:10.1088/1742-5468/2012/06/P06008

Abstract. The particle-scale dynamics of granular materials have commonly been characterized by the self-diffusion coefficient D. However, this measure discards the collective and topological information known to be an important characteristic of particle trajectories in dense systems. Direct measurement of the entanglement of particle space–time trajectories can be obtained via the topological braid entropy S_{braid}, which has previously been used to quantify mixing efficiency in fluid systems. Here, we investigate the utility of S_{braid} in characterizing the dynamics of a dense, driven granular material at packing densities near the static jamming point ϕ_{J}. From particle trajectories measured within a two-dimensional granular material, we typically observe that S_{braid} is well defined and extensive. However, for systems where $\phi \gtrsim 0.79$, we find that S_{braid} (like D) is not well defined, signifying that these systems are not ergodic on the experimental timescale. Both S_{braid} and D decrease with either increasing packing density or confining pressure, independent of the applied boundary condition. The related braiding factor provides a means to identify multi-particle phenomena such as collective rearrangements. We discuss possible uses for this measure in characterizing granular systems.

Keywords: granular matter, mixing, dynamical heterogeneities (experiment)

ArXiv ePrint: 1202.5243

1742-5468/12/P06008+13$33.00

Contents

1. Introduction

Recently, there have been extensive efforts to draw parallels between dense granular systems, foams, emulsions, and glassy molecular systems [1, 2]. For such systems approaching the glass/jamming transition, the dynamics slow down due to an increasing intrication of the available phase space, with rearrangements taking the form of cage jumps [3]–[8]. In this regime, particles are trapped by their neighbors at short timescales and resume diffusive behavior at long timescales due to eventual loss of correlation in the succession of jumps. Such jumps involve cooperatively rearranging regions which induce dynamical heterogeneities [9, 10], and the particles pass each other only rarely. The growth in size of these rearranging regions is believed to be associated with the rigidity and loss of ergodicity exhibited by fragile glasses.

Unlike glassy molecular systems, granular materials permit the tracking of individual particles. The average dynamics have traditionally been characterized by the mean-squared displacement, $\sigma^2(\tau)$. When the experimental timescale is long enough compared to the viscous timescale, permitting a complete decorrelation in the particle motion, it is possible to calculate the self-diffusion constant D. This coefficient is a *single*-particle measure in which all information regarding relative motions of particles is discarded. In contrast, recent experiments and simulations [3, 8], [11]–[18] have shown that the dynamics near the glass transition become heterogeneous in both space and time. As such, it is necessary to take relative motions into account when formulating the correct average description of the state. To this end, *multi*-particle scalars have been developed, including the four-point susceptibility χ_4 [12]–[14]. However, to our knowledge, no scalars have been introduced that characterize mixing effects, which may be relevant to quantifying the cooperative motion of particles.

The central observation of this paper is that the trajectories of a two-dimensional assembly of grains take the form of a *braid* when plotted in a space–time diagram, as shown in figure 2. Each strand of the braid represents the space–time trajectory of a single particle in the system, with the length of the braid corresponding to time and the

J. Stat. Mech. (2012) P06008

entanglement of the strands arising from dynamics. The topological braid entropy, S_{braid}, is a measure of the degree of this entanglement. This approach has been successfully used to analyze the mixing efficiency in two-dimensional fluid flows [19]–[24]. Specifically, the degree of Lagrangian chaos created by the motion of rods in a fluid is quantitatively related to the topology of the corresponding braid. We anticipate that this notion might also be applicable to characterizing caging and dynamical heterogeneity in granular systems, by providing a quantitative measure of how close a system is to departing from ergodicity.

Here, we experimentally investigate the behavior of the average topological braid entropy extracted from the long-time dynamics of particles in a dense, driven granular material, examining the dependence on boundary conditions (constant pressure, CP, and constant volume, CV) and the inter-particle friction coefficient μ. We analyze the dynamics with two methods: a single-particle method (the self-diffusion constant, D) and a *topological* multi-particle method (the braid entropy, S_{braid}). We find that both D and S_{braid} are sensitive to the packing density ϕ and pressure P of the system in the same qualitative way. However, at high ϕ and P, both D and S_{braid} are inaccessible due to insufficiently long experimental timescales or ill-definedness. In contrast, the *braiding factor* can be readily computed, with computational expense comparable to the diffusion coefficient, and offers an instantaneous view of the magnitude and intermittency of the rearrangements in the system.

2. Experiment

We conduct experiments on a two-dimensional granular assembly supported upon a nearly frictionless horizontal air table and agitated by bumpers around the boundary. The granular material is bi-disperse, consisting of large and small particles with diameter of $r_{\mathrm{L}} = 83.6$ mm and $r_{\mathrm{S}} = 55.8$ mm and mass of $m_{\mathrm{L}} = 8.1$ g and $m_{\mathrm{S}} = 3.5$ g, respectively. The concentration of small/large grains is fixed at $N_{\mathrm{S}}/N_{\mathrm{L}} = 2$, so as to occupy similar areas. The apparatus is shown in figure 1.

The boundary condition and the inter-particle friction μ can be changed for each experimental run. The boundary condition is established by the configuration of the piston ($m_{\mathrm{piston}} = 95\, m_{\mathrm{S}}$). By attaching weights to the piston via a low-friction pulley, the system is confined under constant pressure (CP) with a range of pressures $5.7 < P < 80$ mN m^{-1}. The constant volume (CV) boundary condition is established by fixing the piston to the table, where a range of packing densities $\phi = 0.72$–0.81 is explored by removing units of particles (two small and one large), maintaining the relative concentration. The inter-particle friction is selected by changing the material around the particles' outer edge, with $\mu_1 = 0.1$ for PTFE (Teflon) wrapping, $\mu_2 = 0.5$ for bare polystyrene, and $\mu_3 = 0.85$ for rubber.

Around the boundary, an array of bumpers agitates the system on three sides. Bumpers are triggered pairwise via a computer at a high frequency ($f = 10$ Hz) to keep particles in motion despite energy dissipated in collisions. A triggered pair consists of a bumper and its corresponding bumper on the opposite wall. We have previously measured [25] that the effect of this driving system is to provide a thermal-like bath which maintains the granular material at constant average kinetic energy. More information on the driving and kinetics of the system can be found in [25]–[27].

Images are taken $\tau_{\mathrm{camera}} = 2$ or 5 s apart depending on the ϕ-dependent dynamical timescales [26]. We record the positions of particles and map trajectories in time using

J. Stat. Mech. (2012) P06008

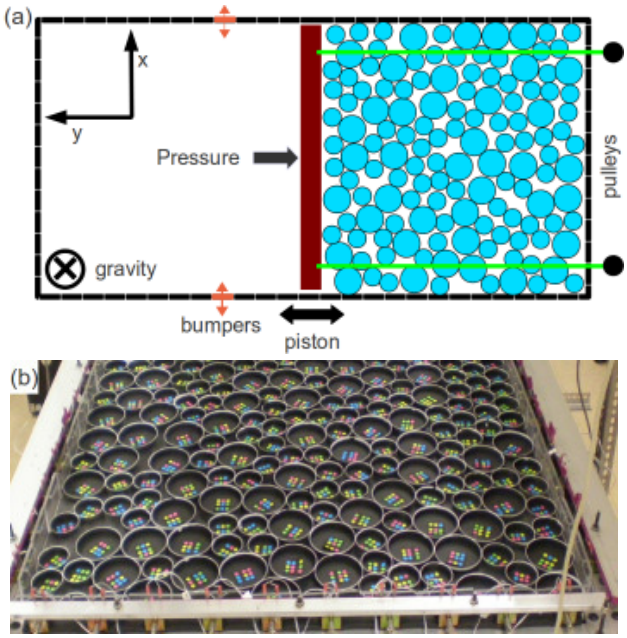

Figure 1. (a) Schematic and (b) photograph of apparatus. The piston provides constant pressure via pulleys and weights, or constant volume by fixing its position to the surface of the table.

unique particle identifiers [26]. The unique identifiers allow a relatively large τ_{camera}, so we can confidently track the trajectories of individual particles and thereby be certain that topological dynamics do not erroneously result from the exchange of particle identities due to tracking mistakes. The packing density ϕ is calculated as $\phi = \langle \pi r_i^2 / V_i \rangle_i$, where r_i the particle radius and V_i its local Voronoi cell area, calculated with Voro++ [28]. The average is taken over all particles in the central 20% area of the table to reduce ordering effects induced by the boundaries [25, 29].

3. Results

3.1. Self-diffusion

The diffusion behavior is quantified using the mean-squared displacement

$$\sigma^2(\tau) = \langle \Delta x_i(t_j + \tau)^2 + \Delta y_i(t_j + \tau)^2 \rangle_{i,j} \tag{1}$$

where the average $\langle \cdot \rangle$ is performed over all particles i and all times t_j. As can be seen in figure 3, the slope of $\sigma^2(\tau)$ is not constant for all timescales τ. It is useful to define a local curve $\sigma^2(\tau) \propto \tau^\alpha$, where the value of α characterizes the average individual dynamics associated with that τ. For short timescales ($\tau < \tau_{\text{D}}$), the trajectories remain sub-diffusive, with $\alpha < 1$. This arises because the particles are locally confined, or caged, by neighboring particles [3, 4]. At longer timescales ($\tau > \tau_{\text{D}}$), each particle has experienced multiple cage-breaking events and thus resumes diffusive behavior. For timescales at which $\alpha = 1$, we can measure the two-dimensional self-diffusion coefficient $D = \frac{1}{4}(\text{d}/\text{d}\tau)\sigma^2(\tau)$. Finally, if the diffusion process is fast enough, a typical particle covers a distance of many particle

J. Stat. Mech. (2012) P06008

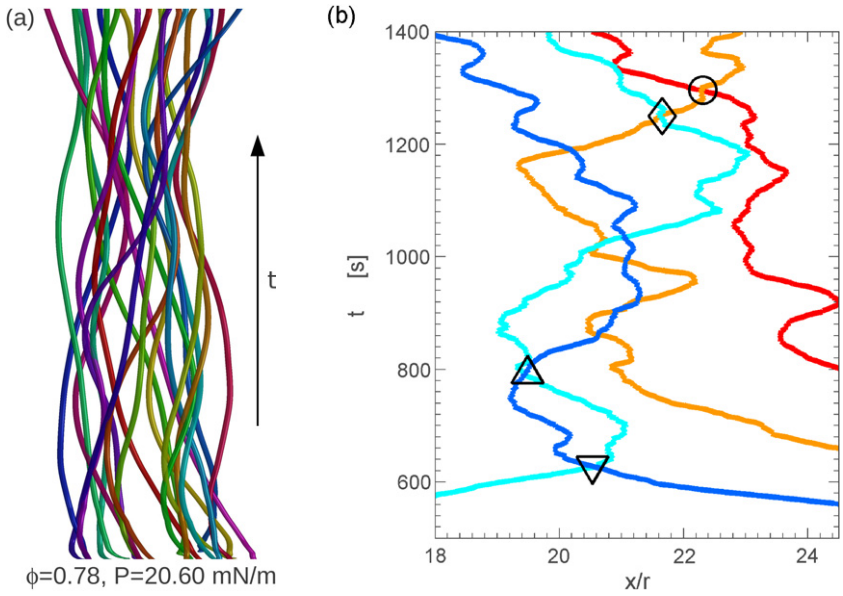

Figure 2. (a) Entanglement of space–time trajectories for $N = 20$ particles, which are (b) projected on the x-axis with four crossings marked with symbols. The crossings ○ and △ are topologically 'over' (left over right), and the crossings ♢ and ▽ are topologically 'under' (left under right). Note that the crossings ▽ and △ undo each other, while ♢ and ○ do not.

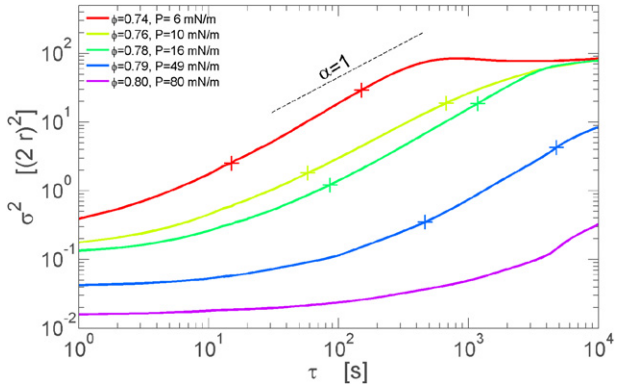

Figure 3. Representative diffusion relations $\sigma^2(\tau)$ for constant pressure (CP) experiments with μ_2 and $\phi = 0.74$–0.80. The dashed line represents a slope of unity. The diffusion coefficient, D, is calculated between the two + symbols on each curve.

diameters within the duration of the experiment. In such cases, the exponent α can again fall below unity at long times, due to the finite size of the experiment. This effect is visible in figure 3 for the lowest ϕ at which we perform experiments.

In general, it is possible to calculate D using $\sigma^2(\tau)$ for experiments which are of long enough duration to reach the $\alpha = 1$ regime. For this system, we find that this regime is reached even at values of ϕ near static random loose packing [26]. A convenient means to measure D is to specify a tolerance on α which defines a diffusive regime, marked by +

symbols in figure 3. We calculate D by fitting to the largest continuous region where the smoothed derivative of $\sigma^2(\tau)$ has a slope $|\alpha - 1| < 0.1$. The diffusive timescale τ_{D} is the timescale at which the particle motion first achieves diffusive behavior. With increasing packing density ϕ, τ_{D} becomes longer, as seen in figure 3. For systems with large ϕ and P, the range of τ over which $\sigma^2(\tau)$ was used to find D (marked with crosses in figure 3) becomes less than a decade.

Given the constraint that $|\alpha - 1| < 0.1$ and the finite duration of our experiment $\approx 10^4$ s, it is not always possible to calculate a diffusion constant for systems with large P or ϕ. One such example ($\phi = 0.80$, $P = 80$ mN m^{-1}) is shown in figure 3. A more conservative tolerance specification on α would further decrease the experiments for which we could calculate a meaningful value of D. In many experiments where we would wish to quantify the self-diffusion of particles, D is in fact poorly defined.

3.2. Braid entropy

The braid entropy is a quantitative measure of mixing, by means of the *degree of entanglement* of trajectories [20, 22, 23]. To illustrate this notion of entanglement, one can think of the means by which three strands of hair can be plaited. The starting configuration of this braiding process is three, unentangled parallel strands, with upper ends attached and bottom ends at positions labeled 1, 2 and 3. Braiding in this context proceeds with two alternating moves: first, the strand in position 1 is passed above the strand in position 2, and second, the strand now in position 2 is passed below the one in position 3. The result is a regular braid. From a mathematical point of view, these moves correspond to group elements, the *over* and *under* moves being the mathematical inverse of one another for a given pair of neighboring strands. The corresponding *braid group* can be similarly defined for an arbitrary number of strands; formal details of the group structure can be found in [30] or most textbooks on knot theory. Importantly, the length of the resulting braid is not specified only by the number of moves, since successive over/under moves can in fact cancel each other. An example of this situation is shown by the triangular symbols in figure 2.

We will quantify the topological notion of entanglement by computing the *braiding factor* L for each sequence. To gain a better physical insight into the meaning of this quantity, one can think about it in the following way. Consider an imaginary rubber band enclosing the strings at the bottom of the braid shown in figure 2(a). As we slide the rubber band upwards along the strands, its length $L(t)$ will tend to grow, as it is caught on the strings and is not allowed to traverse them. The ratio of $L(t)$ to the initial length of the rubber band (which we can assume is one) is the braiding factor. If the trajectories are chaotic, they will build up a non-trivial braid, and $L(t)$ will grow exponentially. The growth rate is then related to the largest Lyapunov exponent of the underlying dynamical system.

The braid entropy S_{braid} is defined as the asymptotic growth rate of $\log L(t)$,

$$S_{\mathrm{braid}} = \lim_{t\to\infty} \frac{\mathrm{d}}{\mathrm{d}t} \log L(t), \tag{2}$$

where $L(t)$ is maximized over the choice of our imaginary rubber band. (We describe below how the rubber band is in practice encoded symbolically.) This rubber band viewpoint is well illustrated by taffy pullers and dough-kneading devices, where material is made to

J. Stat. Mech. (2012) P06008

stretch exponentially by repeated folding [31]. The braid entropy provides a measure of how efficiently the dynamics mixes the system: the characteristic timescale of mixing is proportional to $1/S_{\text{braid}}$.

When trajectories arise from a continuous dynamical system, then the braid entropy is a lower bound on the *topological entropy* of the system. The topological entropy is a measure of the loss of information about the identity of trajectories—it is an entropy in the sense of information theory. As more trajectories are included, the braid entropy converges to the topological entropy [32]. However, in a granular medium such as the one considered here there is no underlying continuous dynamical system: the braid entropy is not necessarily related to some intrinsic topological entropy.

We follow the method described in [23] to calculate a good approximation to the braid entropy, using a symbolic approach based on earlier work [33, 34]. By projecting 2D trajectories along a single axis, as shown in figure 2, we can find all times at which any two particle trajectories cross along the chosen axis; these times are specified as the crossing times. At each crossing, the particle initially on the left passes either over or under the trajectory of the particle initially on the right and the crossing is given a sign of ± 1, respectively. The corresponding algebraic representation is a sequence of braid group generators, with one generator per crossing. The sequence contains all of the information necessary to re-generate the braid projected along the chosen axis. A hypothetical loop (corresponding to the rubber band described above) drawn around the braid and acted upon by the generators will grow in length as a function of time. This can be used to compute the braiding factor $L(t)$, using a purely symbolic description of the loop. This symbolic description relies on the fact that two-dimensional loops can be expressed succinctly in terms of the number of crossings with fixed reference lines, and that an action of the braid group on these coordinates can be defined. Sample code to compute the braiding factor is provided in [23].

We calculate the braiding factor $L(t)$ using the trajectories of $N = 20$ particles. Because particles can enter and leave the region captured by the camera, this choice of number provides a compromise between having too many particles with missing points in the trajectory, and too few particles with the maximum trajectory duration. We find that this choice of N is sufficient for $L(t)$ to capture the dynamics of the whole system, as will be discussed in more detail below.

The braid entropy S_{braid} (see equation (2)) is measured from the growth rate of the logarithm of the braiding factor. To obtain a single value for a particular run, we calculate a linear fit to $\log L(t)$. This entropy will be well defined if $\log L(t)$ meets three conditions: it grows linearly in time, is an extensive quantity, and is independent of the choice of projection axis. We can directly check each of these conditions.

In figure 4, we show $\log L(t)$ for systems identical to figure 3, omitting the system with $\phi = 0.80$ and $P = 80$ mN m^{-1} as too few persistent crossings occur. We find $\log L(t)$ grows, on average, linearly with time for $\phi \lesssim 0.79$. In the inset, $\log L(t)$ is divided by its value at the maximum time, to highlight how the degree of linearity present at different values of ϕ.

To test the extensivity of S_{braid}, we repeat the calculation described above for different numbers of particle trajectories, and test whether S/N is a constant. Figure 5 shows the results of this test for a series of CP experiments at different ϕ. For $N \gtrsim 15$, we observe that S/N is quite flat, independent of boundary condition, μ, ϕ, and P. This

J. Stat. Mech. (2012) P06008

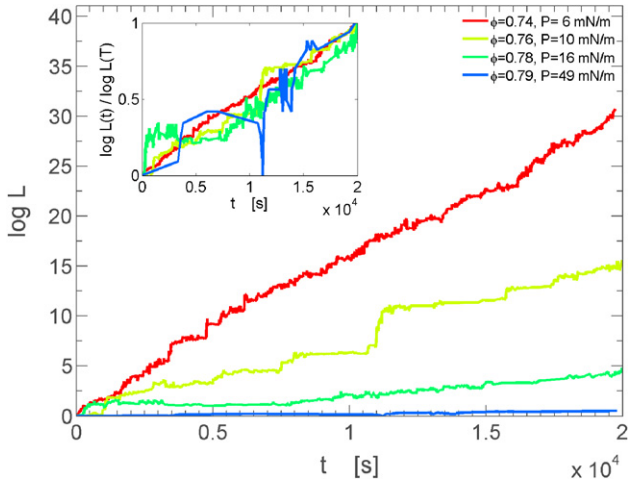

Figure 4. The braiding factor $\log L(t)$ for the same experimental runs shown in figure 3, with $\phi = 0.74$–0.79. The inset shows $\log L(t)$ divided by its value at the maximum time, T.

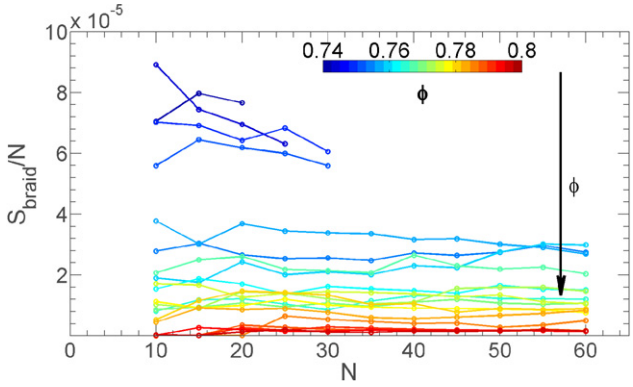

Figure 5. The S_{braid} per particle, shown for μ_2 and CP systems, with the axis of projection $\theta = 0$. The arrow shows increasing ϕ of the system.

observation is consistent with S_{braid} being an extensive quantity. For very small ensembles of trajectories, $N \lesssim 15$ (less than 10% of the system size), we find that the braid is too sparse to be representative of the dynamics of the system. In addition, it is difficult to test for extensivity in systems with low ϕ. In this regime, particles have a larger diffusion constant and are therefore more likely to enter and leave the region being monitored by the camera. Therefore, it is not possible to find $N \gtrsim 25$ particles which all satisfy the constraint on the minimum duration of continuous trajectories required to make a calculation of S_{braid}.

We compute $L(t)$ for 9 projections along axes oriented from $\theta = 0$–$\pi/2$, and compare the results in figure 6 for two characteristic systems, both confined at CP and with μ_2 but at different ϕ and P. For the example at low ϕ, we observe that $\log L(t)$ is quite linear, even on short timescales, and that the choice of projection axis has little effect on the slope of $\log L(t)$ or S_{braid}. However, in the higher-ϕ example, $\log L(t)$ grows more quickly for the $(\theta = \pi/2)$-projection than for the $(\theta = 0)$-projection, where the difference

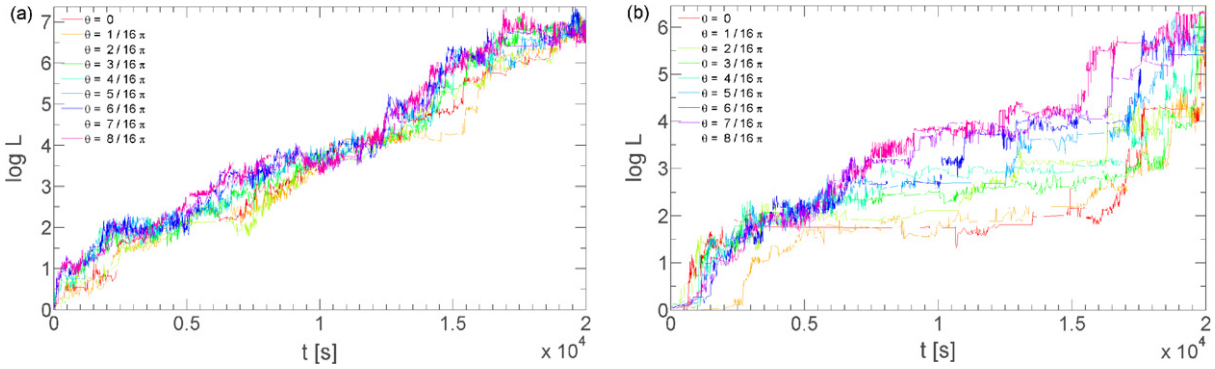

Figure 6. A plot of $\log L(t)$ for two systems with μ_2 where the axis of projection is rotated between $\theta = [0, \pi/2]$, where (a) is $\phi = 0.77, P = 12$ mN m^{-1} and (b) is $\phi = 0.78, P = 18$ mN m^{-1}.

in entropy is ≈2%. Increasing N decreases the difference in entropy between projections. In the limit of long experiment duration, such differences in calculated entropies would be expected to vanish.

In examining the runs at large ϕ and large P, we note the occurrence of two important features in $\log L(t)$ which are not present in the diffusion measurements: flat regions and steep increases. In figure 6(b) (representative of such systems), we observe that $\log L(t)$ may remain constant for an extended period of time, as in this case for the interval $0.7 \lesssim t \lesssim 1.2 \times 10^4$ s. Such a flat $L(t)$ curve signifies that particles are *not* exchanging neighbors. The second feature to note in figure 6(b) is the sharp increases in $\log L(t)$ beginning around $t \approx 1.5 \times 10^4$ s, for all choices of projection axis. Such steps correspond to a large number of crossings, no matter the chosen orientation, and therefore unambiguously signify a *collective rearrangement* of particles (cage-breaking event). Another such event can be seen in figure 4 just after $t = 1 \times 10^4$ s. Due to these events, the slope of $\log L(t)$ can be much larger on short timescales. As such, the assumption that $\log L(t)$ grows linearly in time is *not* valid for short timescales. However, we find S_{braid} is well defined for systems where ($\phi \lesssim 0.79$, $P \lesssim 50$) as $\log L(t)$ is linear on the experimental timescale, extensive, and independent of axis of projection.

3.3. Comparison

Based on prior work [4, 26, 35], we expect D to decrease as ϕ increases. Indeed, in figures 7(a) and (b), D decreases with increasing ϕ and P, independent of boundary condition (CP and CV). Similarly, we find that S_{braid} decreases with increasing ϕ and P, as shown in figures 7(c) and (d), respectively. Error bars represent the average standard error of S_{braid} from the set of nine projections on axes oriented from $\theta = 0$ to $\pi/2$, where the magnitude of the standard error of S_{braid} is ≈10% and does not depend on ϕ and P. We observe little dependence on the inter-particle friction coefficient μ on D and S_{braid}, though qualitatively D decreases with increasing μ.

As discussed earlier, an experimental measurement of D using σ^2 requires a constraint on the value of α to be used to find D, which was selected to be $|\alpha - 1| < 0.1$. For systems

J. Stat. Mech. (2012) P06008

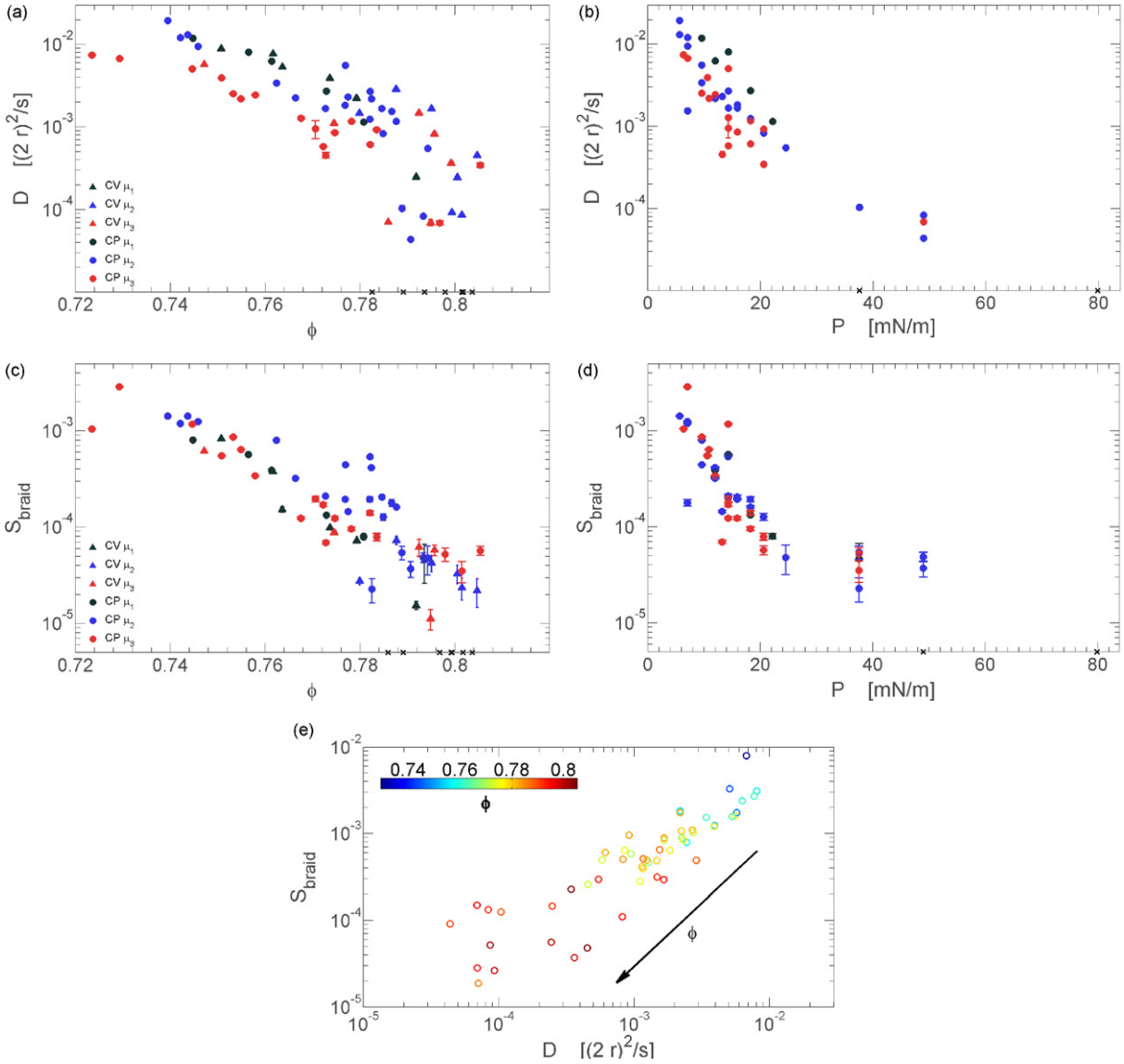

Figure 7. Measured values of D as a function of ϕ and P in (a) and (b), and likewise S_{braid} as a function of ϕ and P in (c) and (d), respectively. Error bars denote the magnitude of the standard error. The black $\times$ on the axis signifies systems for which D or S_{braid} is poorly defined for that particular ϕ or P. (e) A logarithmic plot of S_{braid} and D for each system, where the arrow denotes increasing ϕ.

with high P, this constraint was not met and therefore D is poorly defined, as shown in figures 7(a) and (b). Similarly, S_{braid} is also poorly defined for high P systems as $\log L(t)$ no longer grows linearly within the experimental timescale. For systems with $\phi \gtrsim 0.79$ and $P \gtrsim 50$ mN m^{-1}, neither D nor S_{braid} are useful for measuring the dynamics even with long experimental timescales of 5×10^4 s ($\approx$14 h).

J. Stat. Mech. (2012) P06008

4. Discussion and conclusion

We have investigated the behavior of the global braid entropy S_{braid} associated with the long-time dynamics of a dense granular assembly, and find it to be a well-defined quantity. Notably, S_{braid} was observed to be extensive, making it a promising candidate to play a role in the elaboration of a proper equation of state for dense granular systems. The breakdown in the measurement of S_{braid} coincides with the loss of diffusive dynamics, which is to be expected due to the association of the onset of caging behavior with a loss of ergodicity. The measurement of both S_{braid} and the single-particle diffusion coefficient D provide a quantitative measure of the degree to which slower individual dynamics also results in poorer mixing. In spite of the fact that D is a single-particle measurement, we find that it is a good predictor of the degree of mixing. One benefit of characterizing the average dynamics with S_{braid} instead of D is that no arbitrary fitting parameters, such as α, which is used to identify the diffusive regime, are necessary: the method is instead fully specified by the trajectories themselves.

In addition to providing a measure of the average behavior, the braiding factor $L(t)$ provides a simple way to identify temporal events governing the dynamics, via the crossings. This information is unavailable to single-particle measurements such as D. While there are a few methods available in the literature to identify collective motions, the most common of which are four-point correlation functions, these are computationally costly, slowly converging, and averaged in space and time. In comparison, $L(t)$ is less computationally demanding and provides an instantaneous measurement. We observe that it displays increasing intermittency as the packing density or pressure is increased, with successions of plateaus and jumps indicative of collective neighborhood changes, or structural rearrangements. In fact, this departure from linearity can provide a measure of the chaoticity/ergodicity of the dynamics. The duration required to reach an acceptable degree of linearity, independent of projection axis, is a measurement of a characteristic dynamical timescale of the system. From this point of view, the experimental timescales over which we have investigated our dense granular systems were comparable or larger than this equilibration time, with the exception of the highest P and ϕ systems we tested. For our experimental timescale, a loss of ergodicity was observed for systems with close proximity to the static jamming transition. The size of each jump is likely a function of the number of particles participating in the collective event.

This investigation represents a first step towards a more systematic and controlled characterization of the braid entropy in two-dimensional granular systems. The braiding factor $L(t)$ may be a means of obtaining system trajectories which could be analyzed with the recently developed thermodynamics of histories [36]. Quantitative benchmarking of S_{braid} in thermal and glassy systems, together with a complete comparison with the usual dynamical susceptibilities, are promising directions for future investigations. Extensions to three-dimensional flow may also be possible, by projecting along a plane appropriate to the direction of stirring/shearing.

Acknowledgments

We are grateful to the National Science Foundation for providing support under grant numbers DMR-0644743 (JGP and KED) and DMS-0806821 (J-LT).

J. Stat. Mech. (2012) P06008

References

[1] Liu A J and Nagel S R, *The jamming transition and the marginally jammed solid*, 2010 *Annu. Rev. Condens. Matter Phys.* **1** 347

[2] van Hecke M, *Jamming of soft particles: geometry, mechanics, scaling and isostaticity*, 2010 *J. Phys.: Condens. Matter* **22** 033101

[3] Weeks E R, *Three-dimensional direct imaging of structural relaxation near the colloidal glass transition*, 2000 *Science* **287** 627

[4] Weeks E R and Weitz D, *Properties of cage rearrangements observed near the colloidal glass transition*, 2002 *Phys. Rev. Lett.* **89** 095704

[5] Pouliquen O, Belzons M and Nicolas M, *Fluctuating particle motion during shear induced granular compaction*, 2003 *Phys. Rev. Lett.* **91** 014301

[6] Vollmayr-Lee K, *Single particle jumps in a binary Lennard-Jones system below the glass transition*, 2004 *J. Chem. Phys.* **121** 4781

[7] Marty G and Dauchot O, *Subdiffusion and cage effect in a sheared granular material*, 2005 *Phys. Rev. Lett.* **94** 015701

[8] Reis P M, Ingale R A and Shattuck M D, *Caging dynamics in a granular fluid*, 2007 *Phys. Rev. Lett.* **98** 188301

[9] Cipelletti L and Ramos L, *Slow dynamics in glassy soft matter*, 2005 *J. Phys.: Condens. Matter* **17** R253

[10] Chandler D and Garrahan J P, *Dynamics on the way to forming glass: bubbles in space–time*, 2010 *Annu. Rev. Phys. Chem.* **61** 191

[11] Berthier L, Biroli G, Bouchaud J-P, Cipelletti L, El Masri D, L'Hôte D, Ladieu F and Pierno M, *Direct experimental evidence of a growing length scale accompanying the glass transition*, 2005 *Science* **310** 1797

[12] Dauchot O, Marty G and Biroli G, *Dynamical heterogeneity close to the jamming transition in a sheared granular material*, 2005 *Phys. Rev. Lett.* **95** 265701

[13] Keys A S, Abate A R, Glotzer S C and Durian D J, *Measurement of growing dynamical length scales and prediction of the jamming transition in a granular material*, 2007 *Nature Phys.* **3** 260

[14] Lechenault F, Dauchot O, Biroli G and Bouchaud J-P, *Critical scaling and heterogeneous superdiffusion across the jamming/rigidity transition of a granular glass*, 2008 *Europhys. Lett.* **83** 46003

[15] Candelier R, Dauchot O and Biroli G, *Building blocks of dynamical heterogeneities in dense granular media*, 2009 *Phys. Rev. Lett.* **102** 088001

[16] Candelier R and Dauchot O, *Journey of an intruder through the fluidization and jamming transitions of a dense granular media*, 2010 *Phys. Rev.* E **81** 011304

[17] Duri A, Autenrieth T, Stadler L-M, Leupold O, Chushkin Y, Grübel G and Gutt C, *Two-dimensional heterogeneous dynamics at the surface of a colloidal suspension*, 2009 *Phys. Rev. Lett.* **102** 145701

[18] Candelier R, Widmer-Cooper A, Kummerfeld J, Dauchot O, Biroli G, Harrowell P and Reichman D, *Spatiotemporal hierarchy of relaxation events, dynamical heterogeneities, and structural reorganization in a supercooled liquid*, 2010 *Phys. Rev. Lett.* **105** 135702

[19] Boyland P L, Aref H and Stremler M A, *Topological fluid mechanics of stirring*, 2000 *J. Fluid Mech.* **403** 277

[20] Thiffeault J-L, *Measuring topological chaos*, 2005 *Phys. Rev. Lett.* **94** 084502

[21] Gouillart E, Thiffeault J-L and Finn M D, *Topological mixing with ghost rods*, 2006 *Phys. Rev.* E **73** 036311

[22] Thiffeault J-L and Finn M D, *Topology, braids and mixing in fluids*, 2006 *Phil. Trans.* A **364** 3251

[23] Thiffeault J-L, *Braids of entangled particle trajectories*, 2010 *Chaos* **20** 017516

[24] Allshouse M R and Thiffeault J-L, *Detecting coherent structures using braids*, 2012 *Physica* D **241** 95

[25] Nichol K and Daniels K E, *Equipartition of rotational and translational energy in a dense granular gas*, 2012 *Phys. Rev. Lett.* **108** 018001

[26] Lechenault F and Daniels K E, *Equilibration of granular subsystems*, 2010 *Soft Matter* **6** 3074

[27] Puckett J, Lechenault F and Daniels K, *Local origins of volume fraction fluctuations in dense granular materials*, 2011 *Phys. Rev.* E **83** 041301

[28] Rycroft C H, VORO++*: a three-dimensional Voronoi cell library in* C++, 2009 *Chaos* **19** 041111

[29] Desmond K W and Weeks E R, *Random close packing of disks and spheres in confined geometries*, 2009 *Phys. Rev.* E **80** 051305

[30] Birman J S, *Braids, links, and mapping class groups*, 1975 *Annals of Math Studies* vol 82 (Princeton: Princeton University Press)

[31] Finn M D and Thiffeault J-L, *Topological optimisation of rod-stirring devices*, 2011 *SIAM Rev.* **53** 723

J. Stat. Mech. (2012) P06008

[32] Cox S M and Finn M D, *Two-dimensional Stokes flow driven by elliptical paddles*, 2007 *Phys. Fluids* **19** 113102
[33] Dynnikov I A, *On a Yang–Baxter map and the Dehornoy ordering*, 2002 *Russ. Math. Surveys* **57** 592
[34] Moussafir J-O, *On computing the entropy of braids*, 2006 *Func. Anal. Other Math.* **1** 37
[35] Abate A R and Durian D J, *Approach to jamming in an air-fluidized granular bed*, 2006 *Phys. Rev.* E **74** 031308
[36] Garrahan J P, Jack R L, Lecomte V, Pitard E, van Duijvendijk K and van Wijland F, *First-order dynamical phase transition in models of glasses: an approach based on ensembles of histories*, 2009 *J. Phys. A: Math. Theor.* **42** 075007

J. Stat. Mech. (2012) P06008